SAND REPORT

SAND2002-3828
Unlimited Release
Printed November 2002

A Four-Parameter Iwan Model for Lap-Type Joints

Daniel J. Segalman

Prepared by
Sandia National Laboratories
Albuquerque, New Mexico 87185 and Livermore, California 94550

Sandia is a multiprogram laboratory operated by Sandia Corporation, a Lockheed Martin Company, for the United States Department of Energy under Contract DE-AC04-94AL85000.

Issued by Sandia National Laboratories, operated for the United States Department of Energy by Sandia Corporation.

Available to DOE and DOE contractors from
U.S. Department of Energy
Office of Scientific and Technical Information
P.O. Box 62
Oak Ridge, TN 37831

Telephone:	(865) 576-8401
Facsimile:	(865) 576-5728
E-Mail:	reports@adonis.osti.gov
Online ordering:	http://www.doe.gov/bridge

Available to the public from
U.S. Department of Commerce
National Technical Information Service
5285 Port Royal Rd
Springfield, VA 22161

Telephone:	(800) 553-6847
Facsimile:	(703) 605-6900
E-Mail:	orders@ntis.fedworld.gov
Online ordering:	http://www.ntis.gov/ordering.htm

SAND2002-3828
Unlimited Release
Printed November 2002

A Four-Parameter Iwan Model for Lap-Type Joints

Daniel J. Segalman
Structural Dynamics Research Department
Sandia National Laboratories
P.O. Box 5800
Albuquerque, NM 87185-0847
djsegal@sandia.gov

Abstract

The constitutive behavior of mechanical joints is largely responsible for the energy dissipation and vibration damping in weapons systems. For reasons arising from the dramatically different length scales associated with those dissipative mechanisms and the length scales characteristic of the overall structure, this physics cannot be captured through direct numerical simulation(DNS) of the contact mechanics within a structural dynamics analysis. The difficulties of DNS manifest themselves either in terms of Courant times that are orders of magnitude smaller than that necessary for structural dynamics analysis or as intractable conditioning problems.

The only practical method for accommodating the nonlinear nature of joint mechanisms within structural dynamic analysis is through constitutive models employing degrees of freedom natural to the scale of structural dynamics. In this way, development of constitutive models for joint response is a prerequisite for a predictive structural dynamics capability.

A four-parameter model, built on a framework developed by Iwan, is used to reproduce the qualitative and quantitative properties of lap-type joints. In the development presented here, the parameters are deduced by matching experimental values of energy dissipation in harmonic loading and values of the

force necessary to initiate macro-slip. (These experiments can be performed on real hardware or virtually via fine-resolution, nonlinear quasi-static finite elements.) The resulting constitutive model can then be used to predict the force/displacement results from arbitrary load histories.

Acknowledgment

The author thanks the whole joints research team for providing insight, conjecture, and experimental data that has lead to the developments presented here. The author especially appreciates the collegial and supportive environment provided by his friends. In particular the author thanks his colleague Danny Gregory for providing all the experimental data shown here and his colleague Todd Simmermacher for leading him by the had through the mysteries of elementary Matlab optimization. Dr. Simmermacher also deserves appreciation for reading multiple drafts of this document, making helpful suggestions each time.

Contents

Appendix

Figures

A Four-Parameter Iwan Model for Lap-Type Joints

Introduction

The constitutive behavior of mechanical joints is largely responsible for the energy dissipation and vibration damping in weapons systems. For reasons arising from the dramatically different length scales associated with those dissipative mechanisms and the length scales characteristic of the overall structure, this physics cannot be captured through direct numerical simulation(DNS) of the contact mechanics within a structural dynamics analysis. The difficulties of DNS manifest themselves either in terms of Courant times orders of magnitude smaller than that necessary for structural dynamics analysis or as intractable conditioning problems.

The only practical method for accommodating the nonlinear nature of joint mechanisms within structural dynamic analysis is through constitutive models employing degrees of freedom natural to the scale of structural dynamics. In this way, development of constitutive models for joint response is a prerequisite for a predictive structural dynamics capability.

To be useful, such constitutive models have the following properties:

- They must be capable of reproducing the important features of joint response.
- There must be a systematic method to deduce model parameters from joint-level experimental data or from very fine scale finite element modeling of the joint region.
- Model integration into a structural-level finite element code must be practical.

A framework that has potential for providing that balance is that due to Iwan (1967,1968), and the work reported here addresses how that model-form can be exploited to capture the important responses of mechanical joints.

Iwan introduced constitutive models for metal elasto-plasticity that have since been used to model joints. Of his models, the most prominent has been the parallel system of Jenkins elements, sometimes called the parallel-series Iwan model. As the name implies, such models consist of spring-slider units arranged in a parallel system as indicated in Figure 1.

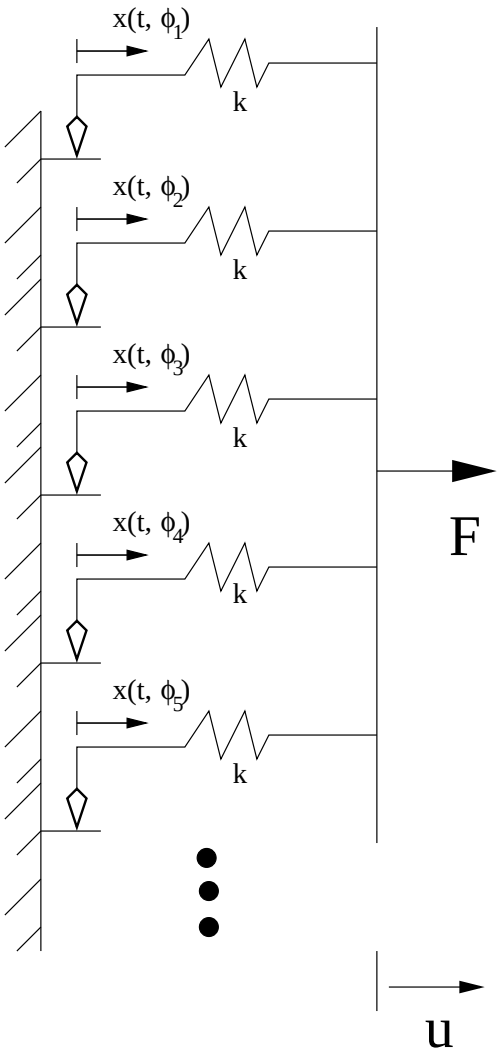

Figure 1. *A parallel-series Iwan system*

Mathematically, the constitutive form of the model is (Segalman, 2001)

$$F(t) = \int_0^\infty \tilde{\rho}(\tilde{\phi}) k[u(t) - \tilde{x}(t, \tilde{\phi})]\, d\tilde{\phi} \tag{1}$$

where u is the imposed displacement,
$F(t)$ is the applied force
$\tilde{\rho}(\tilde{\phi})$ is the population density of Jenkins elements of strength $\tilde{\phi}$
k is the stiffness common to all of the Jenkins elements
and $\tilde{x}(t, \tilde{\phi})$ is the current displacement of sliders of strength $\tilde{\phi}$.

The slider displacements, $\tilde{x}(t, \tilde{\phi})$ evolves from the imposed system displacement, $u(t)$:

$$\dot{\tilde{x}}(t, \tilde{\phi}) = \begin{cases} \dot{u} & \text{if } \|u - \tilde{x}(t, \tilde{\phi})\| = \tilde{\phi}/k \text{ and } \dot{u}\,(u - \tilde{x}(t, \tilde{\phi})) > 0 \\ 0 & \text{otherwise} \end{cases} \tag{2}$$

It is assumed $\tilde{x}(t, \tilde{\phi}) = 0$ initially for all $\tilde{\phi}$. Note that Equation 2 guarantees that $\|u - \tilde{x}(t, \tilde{\phi})\| \leq \tilde{\phi}/k$.

The parameter k can be removed from the above equations through the following changes of variable:

$$\phi = \tilde{\phi}/k \tag{3}$$

$$\rho(\phi) = k^2 \tilde{\rho}(k\phi) \tag{4}$$

$$x(t, \phi) = \tilde{x}(t, k\phi) \tag{5}$$

Equations 1 and 2 now become

$$F(t) = \int_0^\infty \rho(\phi)[u(t) - x(t, \phi)]\, d\phi \tag{6}$$

and

$$\dot{x}(t, \phi) = \begin{cases} \dot{u} & \text{if } \|u - x(t, \phi)\| = \phi \text{ and } \dot{u}\,(u - x(t, \phi)) > 0 \\ 0 & \text{otherwise} \end{cases} \tag{7}$$

We are now guaranteed that $\|u - x(t, \phi)\| \leq \phi$.

The new quantities have different dimensions than the originals. Though $\tilde{\phi}$ has dimensions of force, ϕ has dimensions of length. Similarly, $\tilde{\rho}$ has dimensions of 1/Force but ρ has dimensions of Force/Length^2.

Two overall parameters for the interface can be expressed in terms of the above integral system. The force necessary to cause macro-slip (slipping of the whole interface) is denoted F_S and the stiffness of the joint under small applied load (where

slip is infinitesimal) is denoted K_T. For the parallel-series Iwan system, macro-slip is characterized by every element sliding:

$$u(t) - x(t, \phi) = \phi \tag{8}$$

for all ϕ, so Equation 6 yields

$$F_S = \int_0^\infty \phi \rho(\phi)\, d\phi \tag{9}$$

Similarly for the parallel-series Iwan system, no elements have slid at the inception of loading,

$$x(t, \phi) = 0 \tag{10}$$

at $t = 0$, so Equation 6 yields

$$K_T = \int_0^\infty \rho(\phi)\, d\phi \tag{11}$$

If the joint is subject to cyclic oscillatory deformation, the slope of the hysteresis curve just after reversal has the value K_T, as shown in Figure 2.

Response to Small and Large Force

It is very difficult to obtain meaningful force-displacement information in experiments involving small force amplitudes, but resonance experiments do enable the measurement of dissipation per cycle with reasonable precision. Experiments involving large, monotonically applied forces can provide little detail about joint kinematics, but can indicate the force necessary to initiate macro-slip. It is shown below how each sort of experimental data can be used to determine the parameters of a parallel-series Iwan model that can capture both asymptotic behaviors.

Small Amplitude Oscillatory Loads

When a joint is subject to small amplitude oscillatory lateral loads, the dissipation appears to behave as a power of the amplitude of the applied load. Generally, the exponent of that relationship is a number lying between 2.0 and 3.0. (Goodman pointed out that the Mindlin solution for the energy dissipation resulting from oscillatory lateral loads imposed on two spheres pushed together yields a power-law slope of 3.0 in the regime of small lateral loads.)

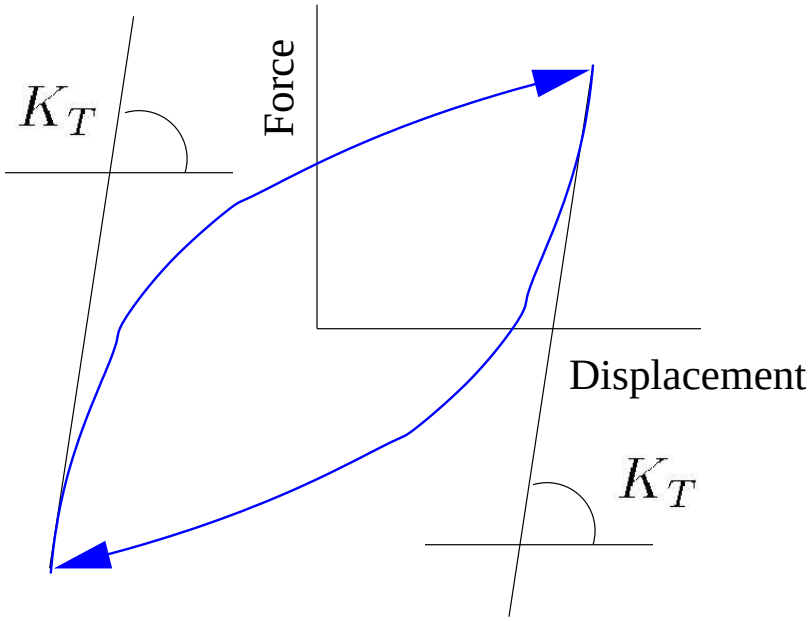

Figure 2. *The joint parameter K_T is the slope of the hysteresis curve immediately after a force reversal.*

In Figure 3, that power-law slope is represented as $3 + \chi$ where χ is a negative number of small magnitude. Mathematically, this is expressed as the following:

$$D(F_0) = \upsilon F_0^{3+\chi} \tag{12}$$

where D is the dissipation per cycle resulting from a harmonic load of amplitude F_0 and υ is an appropriate coefficient.

The dissipation per cycle associated with oscillatory displacements ($u(t) = u_0 \sin(t)$) is slider displacement times the force necessary to cause that displacement, integrated over all Jenkins elements:

$$D = \int_0^{u_0} 4[u_0 - \phi]\phi\rho(\phi)\, d\phi \tag{13}$$

One major simplification made possible for histories where the displacement is bounded by a small value $u_{\max}$ (i.e. $|u(t)| < u_{\max}$) is that the integral of Equations 6 and 7 can be simplified to

$$F(t) = \int_0^{u_{\max}} \rho(\phi)[u(t) - x(t,\phi)]\, d\phi + u(t) \int_{u_{\max}}^{\infty} \rho(\phi)\, d\phi \tag{14}$$

$$= K_T u(t) + O({u_{\max}}^2) \tag{15}$$

where the $O()$ is the notation for quantities that are on the order of their argument as the argument goes to zero [Abromowitz and Stegun, 1964].

Substituting Equation 15 into Equation 13, we see that the dissipation can be written as a convolution involving applied force amplitude:

$$D = \int_0^{F_0/K_T} 4[(F_0/K_T) - \phi]\phi\rho(\phi)\, d\phi \tag{16}$$

$$= 4\ \phi * (\phi\rho(\phi))|_{\phi = F_0/K_T} \tag{17}$$

from which we can conclude that

$$\rho(\phi) = \frac{\upsilon (K_T)^{3+\chi}(2+\chi)(3+\chi)}{4}\, \phi^{\chi} \tag{18}$$

for small arguments of the argument ϕ (Segalman, 2001).

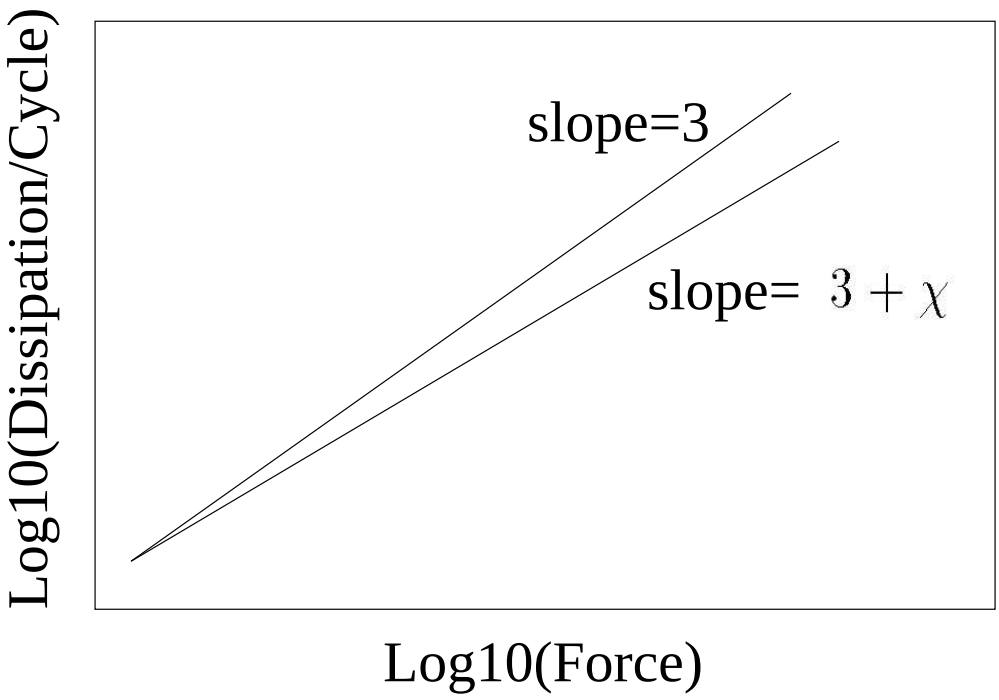

Figure 3. *The dissipation resulting from small amplitude harmonic loading tends to behave as a power of the force amplitude.*

Large Monotonic Loads

Let's consider large monotonic pulls ($0 < \dot{u}$). Equations 6 and 7 show that

$$F(t) = \int_0^{u(t)} \phi\rho(\phi)d\phi + u(t)\int_{u(t)}^{\infty} \rho(\phi)d\phi \tag{19}$$

from which Iwan derived

$$\frac{\partial^2 F(u)}{\partial u^2} = -\rho(u) \tag{20}$$

Because the second derivative of force cannot be measured with any resolution for most joints at small displacements, the above is at best only useful for a large-displacement experiment.

Figure 4 sketches the monotonic force-displacement curve for a canonical lap joint. We anticipate that the force saturates fairly suddenly at F_S and interface displacement u_S. We envision the slope to be nearly discontinuous. Referring to Equation 20 we are inclined to expect that the density $\rho(\phi)$ has finite support and the character of a Dirac delta at the positive end of that support.

Some comment should be made about why we have to guess at the force displacement curves for joints in structures such as we usually encounter. The key observation is that the interface mechanics cannot be viewed directly. The interface region is acted on by external loads through a large elastic region. Additionally, kinematic measurements are of the net displacements of that composite system. Particularly vexing is that the elastic subsystem is generally much more compliant than the interface until the interface has been forced into the vicinity of macro-slip.

This insight is illustrated in Figure 5 showing the monotonic force-displacement curves for a lap joint simulated with an extremely fine mesh. We see that the force is almost linear in displacement until macro-slip suddenly occurs. The nearly linear region is dominated by the compliance of the elastic part of the system; the response of the interface is almost entirely obscured. Once the force is sufficient to cause macro-slip, it is the (near infinite) compliance of the interface which dominates. The conclusion is that for our class of structures, it is very hard to achieve resolution on the force-displacement response of the interface itself through measurements of elastic systems of which the joint is only a small part.

It should be said that for some structures for which the joints represent a major source of stiffness degradation of the structure, Levine and White (2001) were able to deduce Iwan parameters by examining distortion of nominal frequency response

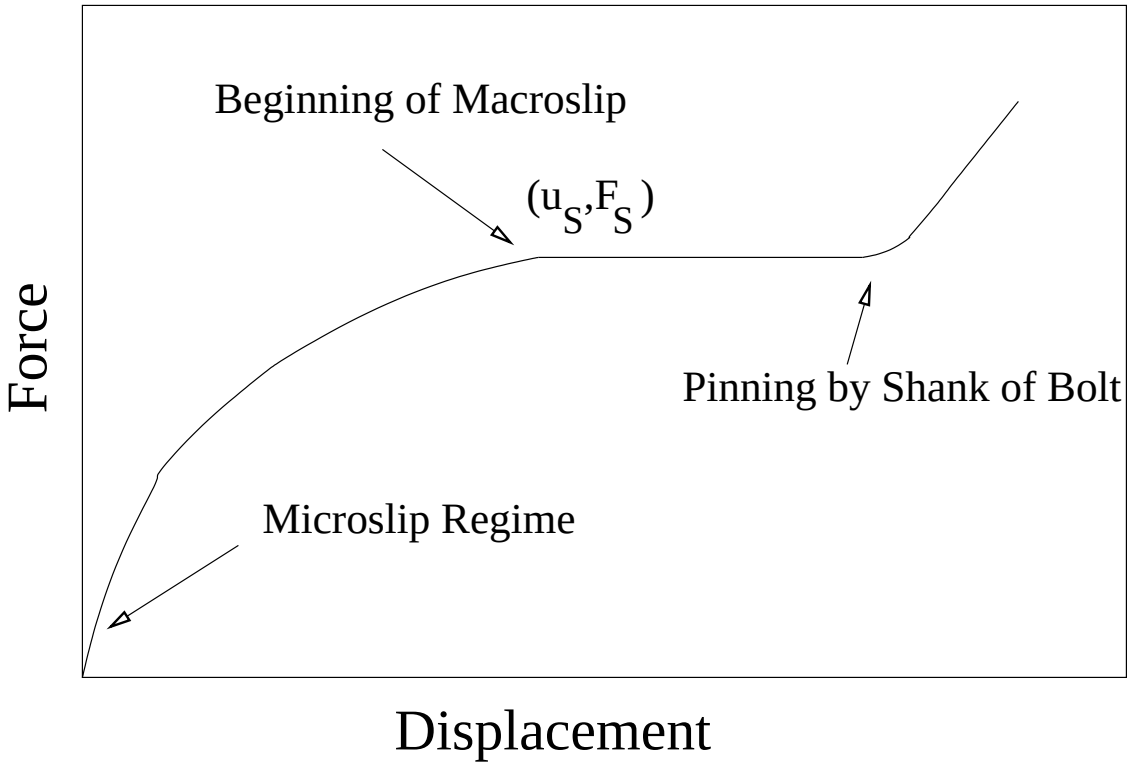

Figure 4. *The monotonic pull of a simple lap joint shows the force saturates at F_S as the displacement passes a critical value.*

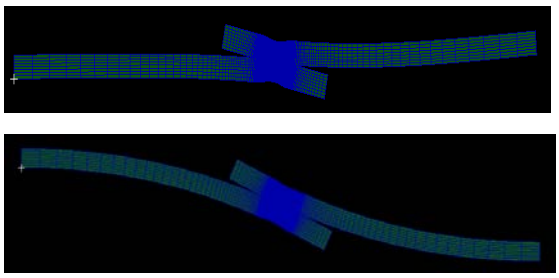

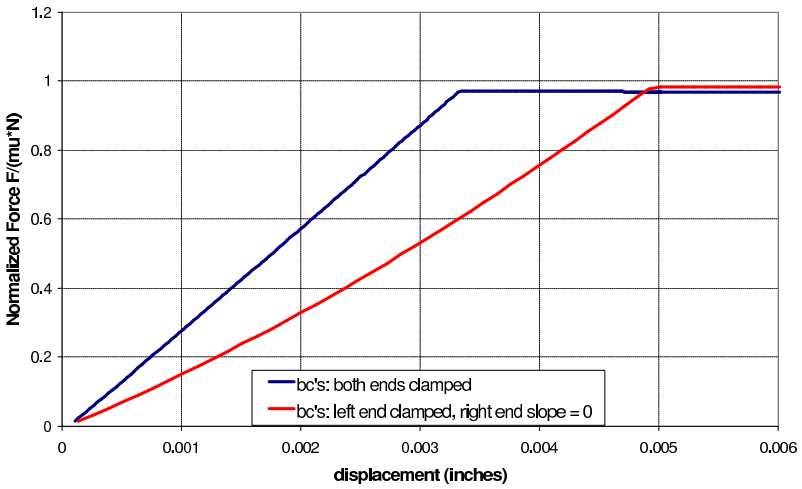

Figure 5. *The numerical predictions of a finely meshed system containing a single lap joint illustrate how interface force and displacements are obscured by the large compliance of the elastic response of the attached members.*

curves as excitation frequency increased. This is an illustration of deducing joint properties indirectly through observation of the integrated behavior of the full structural dynamic response. It is through a similarly indirect approach that parameter estimation is pursued in the following.

Truncated Power-Law Spectra

Given the above observations, we are lead to consider parallel Iwan systems having a power-law population distribution terminated by a Dirac delta:

$$\rho(\phi) = R\phi^{\chi}[H(\phi) - H(\phi - \phi_{\max})] + S\delta(\phi - \phi_{\max}) \tag{21}$$

where $H()$ is the Heaviside step function and $\phi_{\max}$ is numerically equal to u_S. The coefficient S has a value to bring the slope of the monotonic pull curve down to zero at (u_s, F_s). This form of population distribution is shown graphically in Figure 6.

Substitution of Equation 21 into Equation 6 yields

$$F(t) = \int_0^{\phi_{\max}} [u(t) - x(t,\phi)] R\phi^{\chi}\, d\phi + S[u(t) - x(t,\phi_{\max})] \tag{22}$$

Equation 7 remains unaltered.

The macro-slip force for the system becomes

$$\begin{aligned} F_S &= \int_0^{\phi_{\max}} \phi\rho(\phi) d\phi && (23)\\ &= \frac{R\phi_{\max}^{\chi+2}}{(\chi+2)} + S\phi_{\max} && (24)\\ &= \phi_{\max}\left(\frac{R\phi_{\max}^{\chi+1}}{\chi+1}\right)[\frac{\chi+1}{\chi+2} + \beta] && (25) \end{aligned}$$

where

$$\beta = S/\left(\frac{R{\phi_{\max}}^{\chi+1}}{\chi+1}\right) \tag{26}$$

Because χ and β are dimensionless and because F_S can be measured or computed fairly directly, a preferred set of model parameters are $\{\chi, \beta, F_S, \phi_{\max}\}$. For this reason, one inverts Equation 25 to solve for R and employs Equation 26 to express S appropriately:

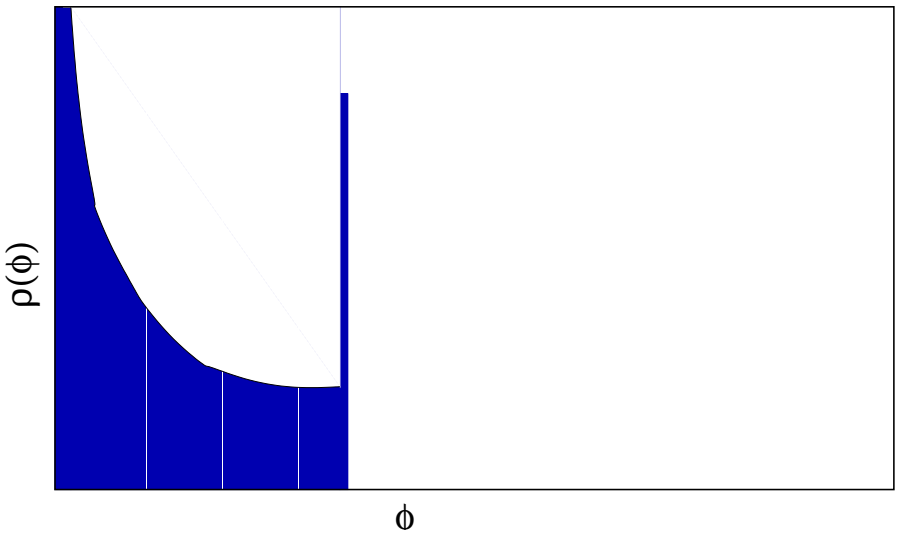

Figure 6. *A spectrum that is the sum of a truncated power law distribution and a Dirac delta function can be selected to satisfy asymptotic behavior at small and large force amplitudes.*

$$R = \frac{F_S(\chi+1)}{\phi_{\max}^{\chi+2}\left(\beta + \frac{\chi+1}{\chi+2}\right)} \tag{27}$$

and

$$S = \left(\frac{F_S}{\phi_{\max}}\right)\left(\frac{\beta}{\beta + \left(\frac{\chi+1}{\chi+2}\right)}\right) \tag{28}$$

The interface stiffness could be computed as

$$K_T = \int_0^{\phi_{\max}} \rho(\phi)d\phi = \frac{R\phi_{\max}^{\chi+1}}{(\chi+1)} + S = \frac{R\phi_{\max}^{\chi+1}}{(\chi+1)}(1+\beta) = \frac{F_S(1+\beta)}{\phi_{\max}(\beta + \frac{\chi+1}{\chi+2})} \tag{29}$$

Oscillatory Response

Because of signal-to-noise problems, there is little data available in the regime of small imposed loads. We are left having to do parameter identification and comparisons

with data from experiments involving large-forces. In particular, we examine large-force oscillatory experiments.

Direct solution of Equations 22 and 7 for a problem specified by $F = F_0 \sin(t)$ would involve solution of a difficult nonlinear integral equation. An alternative approach is to specify $u(t) = u_0 \sin(t)$ and then to solve for the resulting dissipation and peak force.

Noting that the maximum displacement of Jenkins elements of strength ϕ is $x(t, \phi) = u_0 - \phi$, we observe that for $u_0 \leq \phi_{\max}$ the dissipation per cycle of such elements is $4(u_0 - \phi)\phi$. The net dissipation per cycle is

$$D = \int_0^{u_0} 4[(u_0 - x(t, \phi))]\phi\rho(\phi)d\phi \tag{30}$$

This is similar to Equation 16, but no assumption of small displacement is made. For the density function of Equation 22 and for $u_0 \leq \phi_{\max}$, the dissipation per cycle is

$$\frac{4Ru_0{}^{\chi+3}}{(\chi+3)(\chi+2)} = r^{\chi+3}\,\frac{4R\phi_{\max}{}^{\chi+3}}{(\chi+3)(\chi+2)} = r^{\chi+3}\,\frac{4F_S\,\phi_{\max}\,(\chi+1)}{(\beta+\frac{\chi+1}{\chi+2})(\chi+2)(\chi+3)} \tag{31}$$

where $r = u_0/\phi_{\max}$.

Next, we presume that the maximum force seen in each cycle is that force current during the maximum displacement in the cycle.

$$\begin{aligned} F_0 &= \int_0^{u_0} \phi\rho(\phi)d\phi + u_0 \int_{u_0}^{\phi_{\max}} \rho(\phi)d\phi & (32)\\ &= u_0(S + R\frac{\phi_{\max}{}^{\chi+1}}{\chi+1}) - \frac{Ru_0{}^{\chi+2}}{(\chi+1)(\chi+2)} & (33) \end{aligned}$$

Though the above is not a rigorously derived relationship, numerical calculations have shown it to be correct to within numerical precision.

Equation 33 is made non-dimensional by dividing by F_S

$$F_0/F_S = r\,\frac{(\beta+1) - r^{\chi+1}/(\chi+2)}{\beta + (\chi+1)/(\chi+2)} \tag{34}$$

The experimental quantity most easily measured is dissipation (D) as a function of applied lateral load amplitude (F_0). Though these are dimensioned quantities, we

see that all the dimensions drop out when we plot $\partial \log(D)/\partial \log(F_0/F_S)$

$$\partial \log(D)/\partial \log(F_0/F_S) = \frac{\partial D/\partial u_0}{D} / \frac{\partial F_0/\partial u_0}{F_0} \tag{35}$$

$$= (\chi+3)\frac{(S + R\frac{{\phi_{\max}}^{\chi+1}}{\chi+1}) - R\frac{{u_0}^{\chi+1}}{(\chi+1)(\chi+2)}}{(S + R\frac{{\phi_{\max}}^{\chi+1}}{\chi+1}) - R\frac{{u_0}^{(\chi+1)}}{\chi+1}} \tag{36}$$

$$= (\chi+3)\frac{(\beta+1) - r^{\chi+1}/(\chi+2)}{(\beta+1-r^{\chi+1})} \tag{37}$$

Note that as $u_0 \to 0$,

- $F_0 \to u_0(\beta+1)R\frac{{\phi_{\max}}^{\chi+1}}{\chi+1} = u_0 K_T$,
- and $\partial \log(D)/\partial \log(F_0) \to \chi + 3$.

Also, $u_0 \to \phi_{\max}$,

- $F_0 \to F_S$,
- and $\partial \log(D)/\partial \log(F_0) \to (\chi+3)(\beta + \frac{\chi+1}{\chi+2})/\beta$.

In a similar manner, we use the chain rule to calculate the second derivative of the log-log plot:

$$\frac{\partial^2 \log D}{\partial \log(F_0/F_S)^2} = \frac{\frac{\partial}{\partial r}\frac{\partial \log D}{\partial \log(F_0/F_S)}}{\frac{\partial}{\partial r}\log(F_0/F_S)} \tag{38}$$

$$= \frac{r^{(\chi+1)}(\beta+1)(\chi+1)^2(\chi+3)\left[(\beta+1)(\chi+2) - r^{(\chi+1)}\right]}{\left[\beta+1-r^{(\chi+1)}\right]^3(\chi+2)^2} \tag{39}$$

Note that as $\beta \to \infty$, the curvature goes to zero everywhere, but if $\beta = 0$, then the curvature goes to ∞ as $r \to 1$. If β is nonzero, then the curvature is at least bounded.

One last quantity that involves only measurable components on the left hand side, but does retain one dimensioned element on the right hand side is

$$D/F_S = 4\phi_{\max} \frac{r^{\chi+3}}{(\chi+3)} \frac{(\chi+1)/(\chi+2)}{[\beta + (\chi+1)/(\chi+2)]} \tag{40}$$

While Equations 37 and 39 have to do with the shape of the $\log(D)$ vs $\log(F_0)$ curve, Equation 40 is useful in choosing model parameters to match actual *values* of dissipation.

Identifying Parameters

Discussed next are two similar strategies for determining the parameters for the Iwan system discussed above so as to reproduce available experimental data. The first method is more intuitive, and should give some sense of the meaning of each model parameter. The second is automated and more suited to processing multiple sets of experimental data.

One quantity that is assumed known is F_S, through either experiment or finite element analysis. Additionally, it is assumed that dissipation D as a function of applied lateral load amplitude is known over a range of those load amplitudes.

Manual Method

The following strategy for estimating the remaining parameters involves a lot of operator interaction and 'eyeballing', but it appears to be robust. The computational parts are easily implemented in Excel.

1. Plot the experimental values for $\log(D)$ vs. $\log(F_0/F_S)$, and adjust χ and β so that plot of $\log(D)$ vs. $\log(F_0/F_S)$ from Equations 31 and 34 has the same slope and curvature as the experimental curve.

   This is facilitated by generating a column of values of r and corresponding columns of F_0/F_S (Eq. 33) and $D/(R\phi_{\max}^{3+\chi})$ (Eq. 31) and normalizing that curve so that it lies near the experimental data. The user then adjusts χ and β until the curves appear to overlie. If the curvature appears to be approximately zero, choose β to be a number on the order of 10.

2. Employ Equation 34 to deduce the dimensionless displacement amplitude $\hat{r} = u_0/\phi_{\max}$ corresponding to some data point near the center of the experimental data.

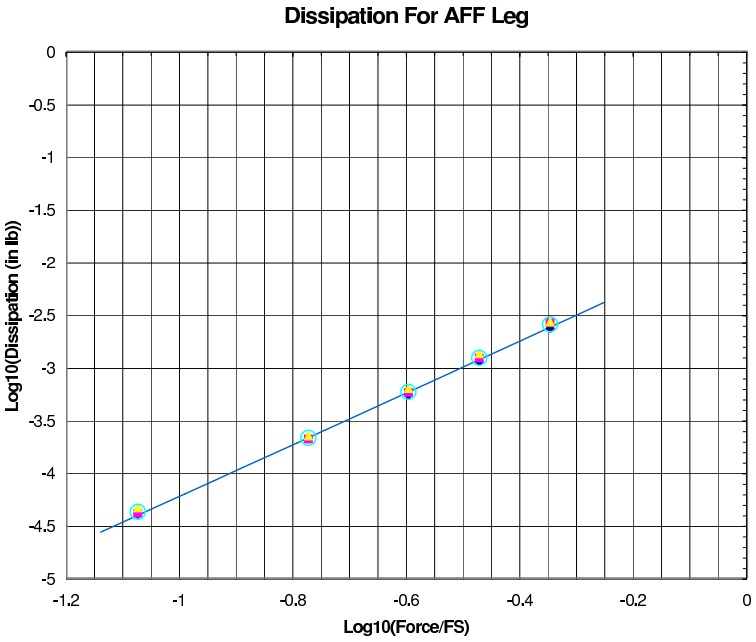

Figure 7. *Fit to dissipation data from a mock W76 AFF leg using the more manual method. The colored points are experimental data, the open circles are centered on the average of the experimental data, and the curve is obtained from a spectrum as described in this report.*

3. Use Equation 40 at that experimental data point to deduce $\phi_{\max}$.

4. R and S are then obtained by evaluating Equations 27 and 26.

The following two figures show reasonable fits to experimental dissipation using the above method. In the first case, (Figure 7) the fit is to data from a bolted leg of a mock AFF (arming-fusing-firing set) (Figure 8) of a mock W76 warhead. (These mock components were manufactured as part of the Campaign 6 experimental program for validating predictive simulation capabilities). We see that the dissipation data appear to lie on a straight line when plotted in a log-log manner. The parameters used to fit that data were: $F_S = 504$, $\phi_{\max} = 7.29\,\text{x}10^{-4}$, $\chi = -0.58$, and $\beta = 10$. These parameters were determined from the loads nominally seen on the plane of the interface. Because the interface is canted 45° from the line of action of the applied loads, the shear forces seen by the interface is the axial load divided by $\sqrt{2}$.

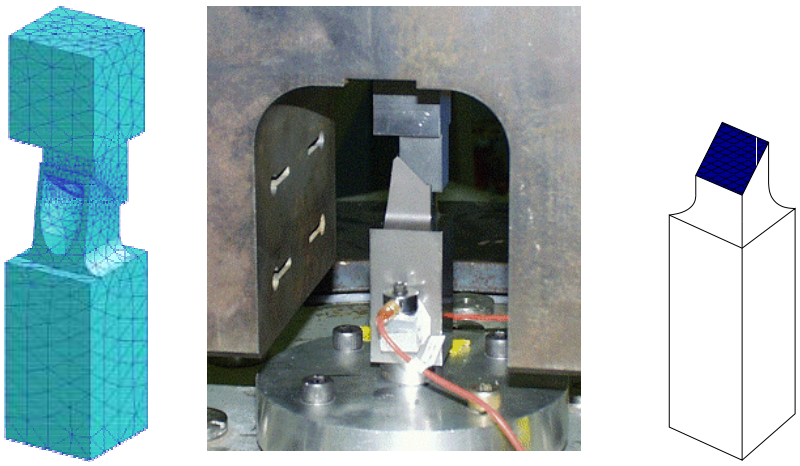

Figure 8. *The leg section of the AFF mock-up. To the left is a finite-element mesh of the full leg section, in the middle is the actual leg section in the test apparatus, and to the right is a sketch indicating the interface being modeled by the 4-parameter model.*

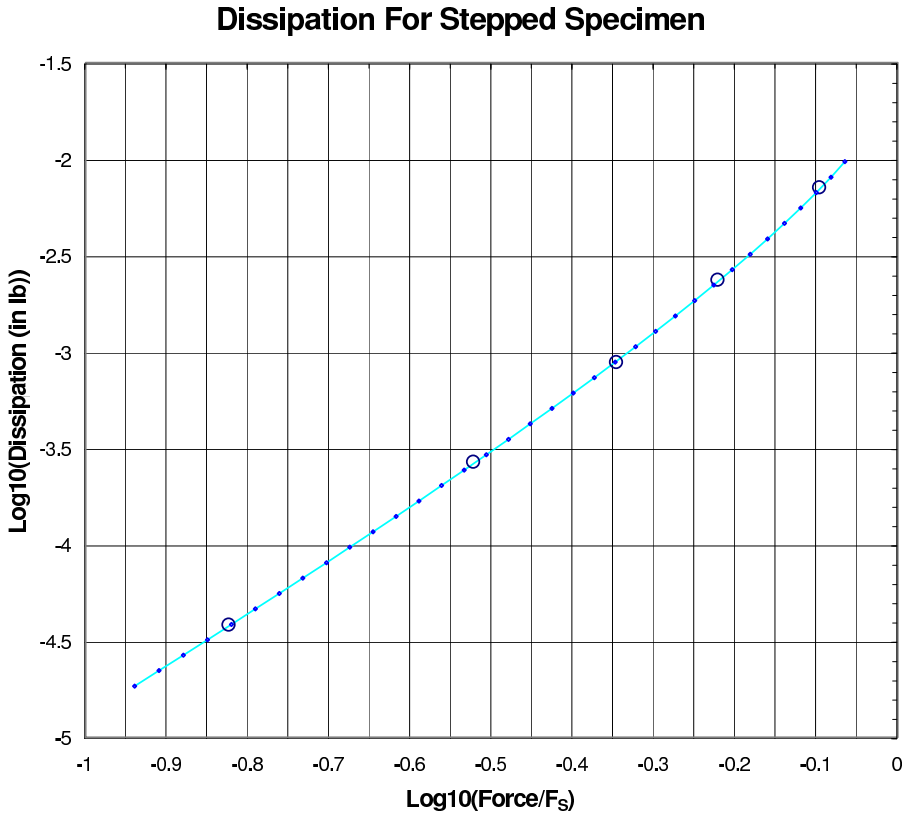

Figure 9. *Fit to dissipation data from a stepped specimen. The open circles are experimental data, and the curve is obtained from a spectrum as described in this report.*

Though the AFF leg problem may appear simple (it is not) because the log-log plot of dissipation vs lateral force is nearly linear, the case of the stepped sample shown in Figure 9 shows substantially more curvature. This result is from a geometrically simple test specimen (Figure 10). The qualitatively different response might be due to the near singular normal tractions at the edges of the contact patch. Reasonably good fit of the 4-parameter model presented above is obtained by setting $F_S = 400$, $\phi_{\max} = 4.92\,\text{x}10^{-5}$, $\chi = -0.6$, and $\beta = 0.1$.

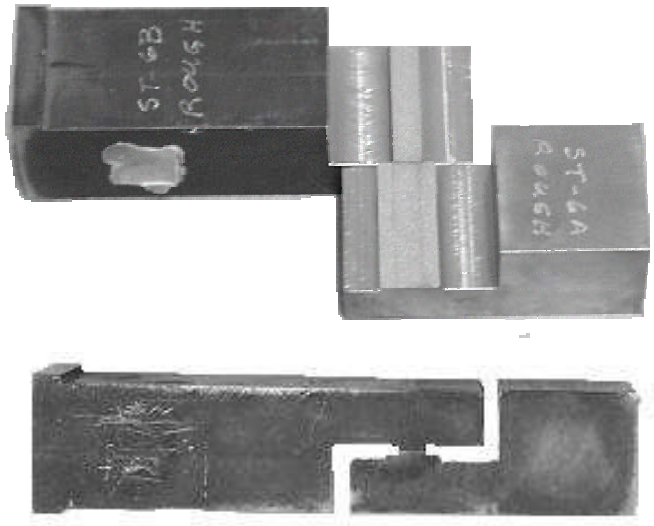

Figure 10. *A stepped specimen shows qualitatively different dissipation than a simple half-lap joint. The difference may be do to the near singular traction that develop at the edges of the contact patch.*

Automated Method

Though the above algorithm might yield to automation, the following algorithm is designed especially to employ Matlab's optimization tools. Matlab's *fminsearch* tool is used to determine χ, β, and $R\phi_{\max}^{\chi+3}$ so as to fit the experimental data points as well as possible. One subtlety is that each comparison of the 4-parameter model with the experimental data requires solution for $r(\chi, \beta, F_0/F_S)$. Once those three parameters are found, the rest of the steps are much as indicated in the previous method. The necessary code is illustrated in the Appendix .

Figures 11 and 12 illustrate the results of this method for the cases considered above. The parameters obtained by the method are indicated in those figures. We see that in each case the more automated method (using Matlab) obtained parameters very similar to those which were obtained in the more manual method, though the automated method does reproduce the experimental data more closely.

Continuity of the Inverse Map

We have seen above that parameters can be found to make the 4-parameter model reproduce experimental dissipation data reasonably well. A further measure of merit of a constitutive model is whether model parameters deduced to fit similar data sets are themselves similar. This issue is addressed here.

We consider dissipation data collected from an AFF leg nominally identical to the one discussed above. The leg was repeatedly disassembled and reassembled and tested between disassembly/reassembly cycles. Nine resulting data sets are shown in Figure 13. We see that eight of those nine data sets lie reasonably close to each other. The data set labeled AFF_4 generates consistently less dissipation.

The Matlab code discussed above maps each data set to a set of four corresponding model parameters. Normalized model parameters deduced using the Matlab tool are shown in Figure 14. The value of F_S is specified at the same value among all data sets, and the Matlab code tends to set $\beta = 10$ when there is little curvature in the log(dissipation)/log(force) curve, so there is variation only in the χ and $\phi_{\max}$ parameters. We see that the values of χ and $\phi_{\max}$ deduced from all the data sets seem to cluster with the exception of the valve of $\phi_{\max}$ deduced from data set AFF_4.

The anomalous nature of the fourth data set is illustrated more strongly by Figure 15, where variability among the experimental data are considered. A variability metric

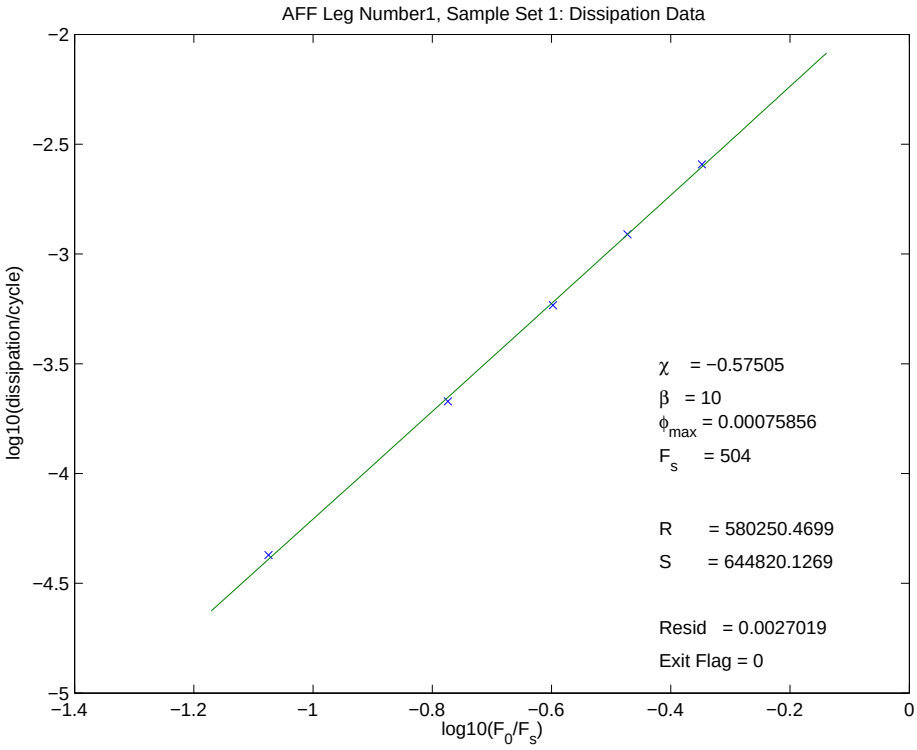

Figure 11. *Fit to dissipation data from a mock W76 AFF leg using the method exploiting Matlab.*

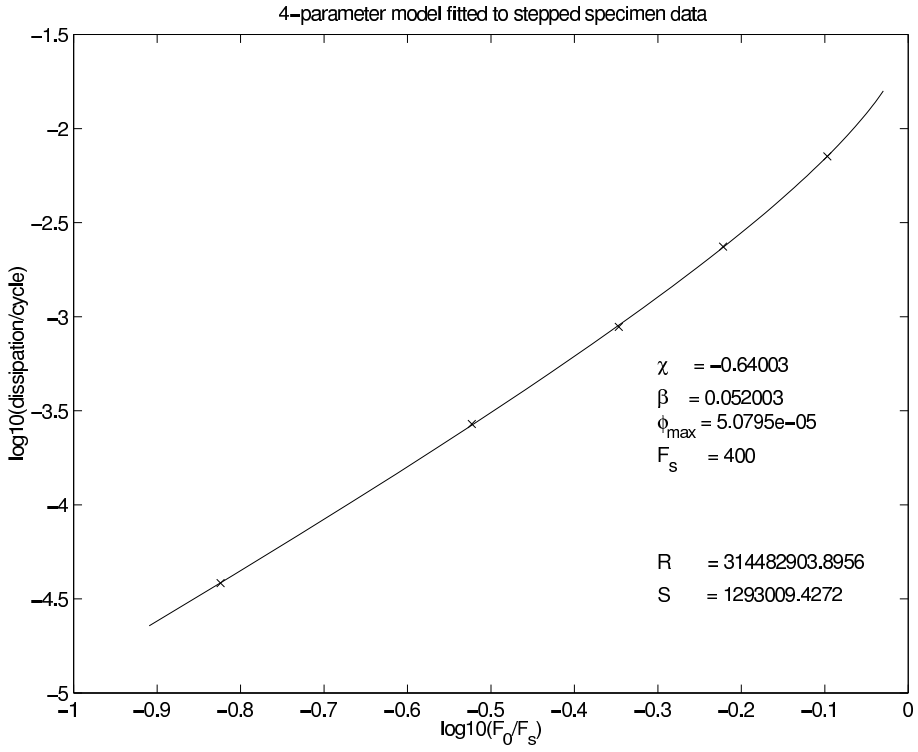

Figure 12. *Fit to dissipation data from a stepped specimen using the method that employs Matlab.*

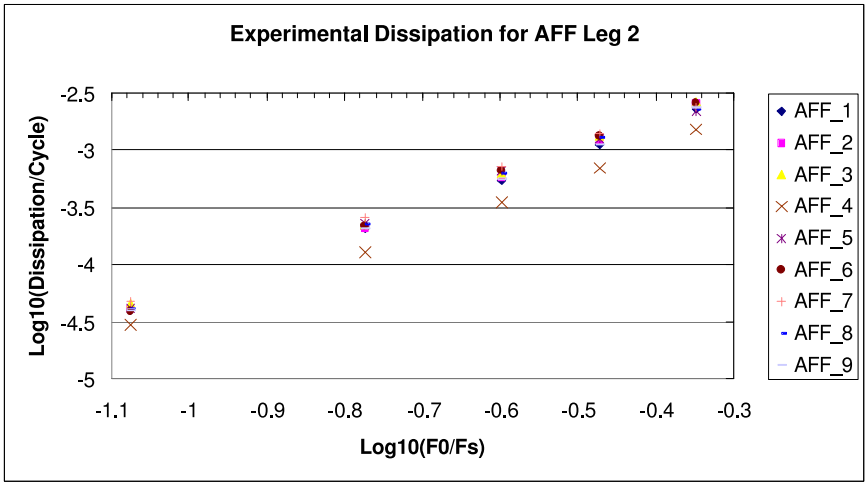

Figure 13. *Experimental dissipation curves measured for a single mock AFF leg that was disassembled and reassembled between tests.*

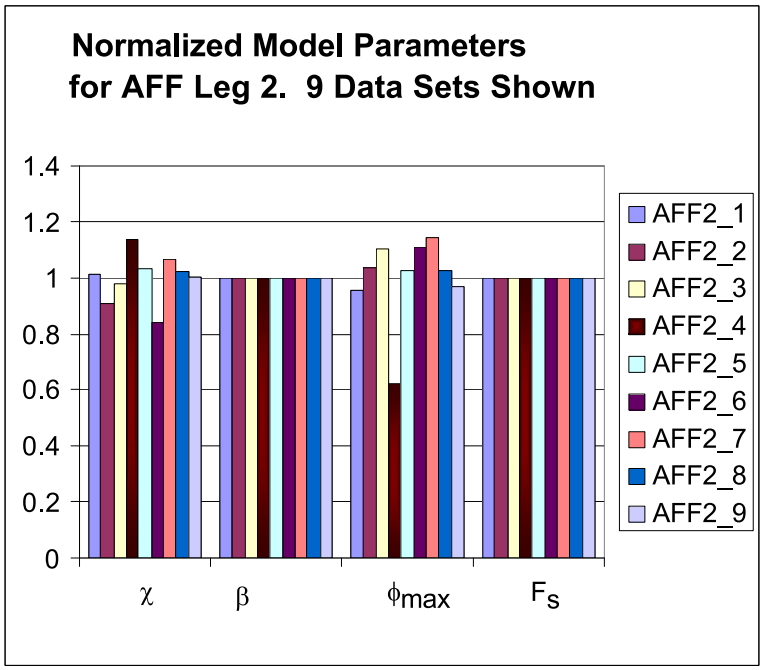

Figure 14. *Parameters for the 4-parameter model determined using Matlab code to fit the above experimental data. To show all parameters on one curve, each parameter was normalized by the average of the parameters deduced from all data sets.*

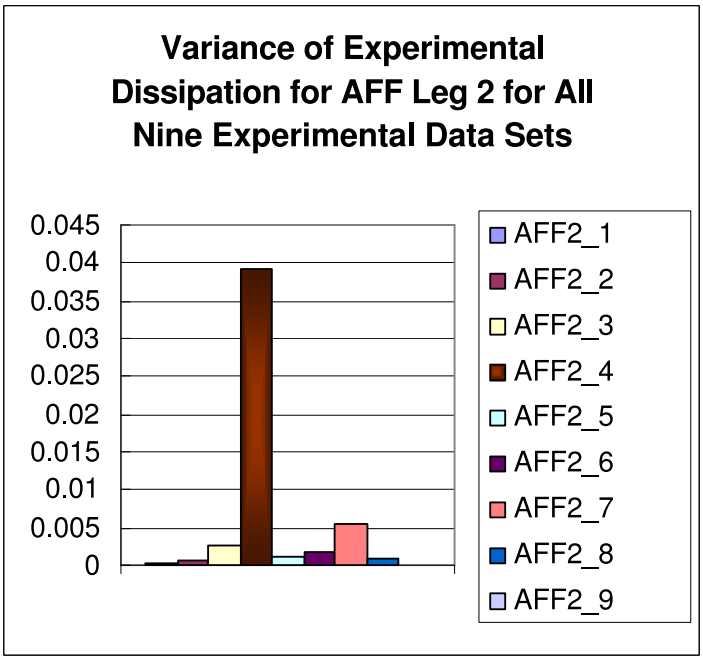

Figure 15. *Variance (calculated using relative error) between the 9 experimental data sets and the experimental mean.*

is defined here in a manner that captures the relative error:

$$V_E^I = \frac{1}{N_{\text{data values}}} \sum_{k=1}^{N_{\text{data values}}} \left[\log(D_k^I/\bar{D}_k)\right]^2 \tag{41}$$

where $\bar{D}_k$ is the kth data value averaged over all the data sets:

$$\bar{D}_k = \frac{1}{N_{\text{data sets}}} \sum_{I=1}^{N_{\text{data sets}}} D_k^I \tag{42}$$

and D_k^I is the kth data value in the Ith data set. We see that the variability of the fourth data set stands out as being approximately ten times the next largest variability. From this point on, we discard that data set and consider only the remaining eight.

The model parameters obtained by averaging the corresponding parameters deduced from each of the remaining eight data sets are reasonably close to those deduced

earlier for an AFF leg. They are $\chi = -0.57245$, $\beta = 10$, $\phi_{\max} = 0.000761268$, and $F_S = 504$.

Figure 16 shows several measures of variability among the remaining eight data sets:

- The variability among the experimental data is shown on the left of the figure. In this case the largest variability is that of case AFF_7 and has a value of approximately 0.0025, corresponding to a disagreement between this data set and the average of the others of approximately 5%.

- The variability of the experimental data from the predictions made by the model when each of the four model parameters is obtained by averaging the corresponding parameters deduced from the eight experimental data sets:

$$V_M^I = \frac{1}{N_{\text{data values}}} \sum_{k=1}^{N_{\text{data values}}} \left[\log(D_k^I/\hat{D}_k)\right]^2 \tag{43}$$

  where $\hat{D}_k$ is the kth data value predicted by the four-parameter model. We see that the variability between the model predictions and the experimental data is on the same order as that found among the experimental data sets themselves.

- A more stringent test of the model's ability to capture the experimental data is to measure the variability between each of the data sets and model predictions made using parameters deduced from all the *other* experimental data sets:

$$V_C^I = \frac{1}{N_{\text{data values}}} \sum_{k=1}^{N_{\text{data values}}} \left[\log(D_k^I/\tilde{D}_k^I)\right]^2 \tag{44}$$

  where $\tilde{D}_k^I$ is the k data value predicted by the four-parameter model using model parameters averaged from quantities deduced from all data sets *except* the Ith. We see that the variability between the model predictions and the experimental data is about 25% larger than that found among the experimental data sets themselves. This is very good consistency.

We conclude from the above that the four-parameter model is capable both of reproducing the data provided to it and of doing so in a consistent manner with systematically deducible parameters.

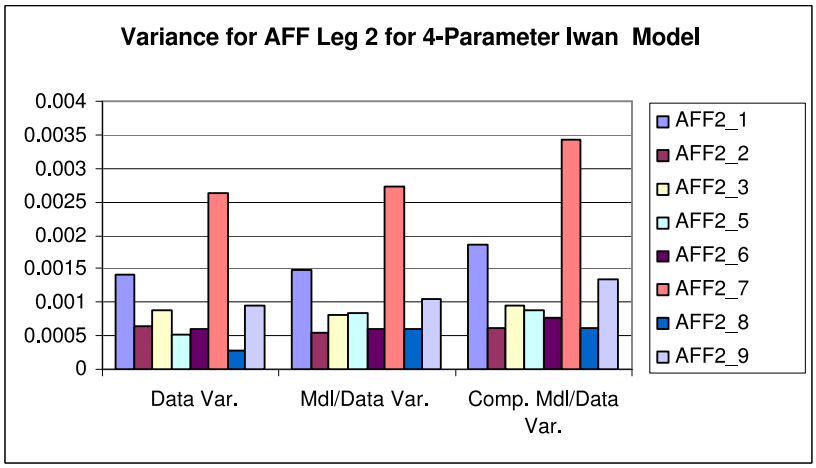

Figure 16. *Variability (calculated using relative error) within the 8 clustering experimental data sets, between the experimental data and that of the nominal model, and between each data set and a model deduced using all the other data sets.*

Power-Law Behavior

Some comment is appropriate about the determination of β (and $\phi_{\max}$) for the case where the curvature of the log-log plot of dissipation versus force amplitude appears to be zero. There is just not enough information in such cleanly power-law behavior to determine the model parameters χ, β, and $\phi_{\max}$. (F_S should be known a priori.) The following is done by both the manual and automated methods under those circumstances:

- β is automatically set to 10;
- χ is uniquely determined by the slope of the log-log dissipation curve;
- F_S is known a priori;
- $\phi_{\max}$ is determined so that - consistent with the above values of χ, β, and F_S - the predicted and measured dissipation are consistent.

If there are experimental or computational values for the stiffness of the system containing that joint, the additional condition can be used to make the determination of the model parameters better posed. In application, that last condition is implemented by asking the Matlab optimization code to make the model stiffness K_T achieve the desired values.

For illustration we consider the AFF leg specimen again. In this instance we devise an equivalent joint model for which all the forces and displacements occur in direction of the line of action of the applied force (Figure 17). Such a joint model might be used in a two degree-of-freedom approximation to a system consisting of the elastic portions of the specimen, the joint, and the reaction mass.

Resonance experiments indicate that the stiffness of the jointed leg is approximately $1.56\text{x}10^6\, lb_f/in$. The stiffness of a similar monolithic (non-jointed) leg is approximately $2.67\text{x}10^6\, lb_f/in$. It would be desirable to be able to adjust β and $\phi_{\max}$ so that K_T in Equation 29 could account for the difference. Alternatively one could set the stiffness of the elastic component of the jointed structure to the full $1.56\text{x}10^6\, lb_f/in$ and select β and $\phi_{\max}$ so that K_T is substantially larger. In either case, we have guidance as to desirable ranges for K_T. The first approach is demonstrated below.

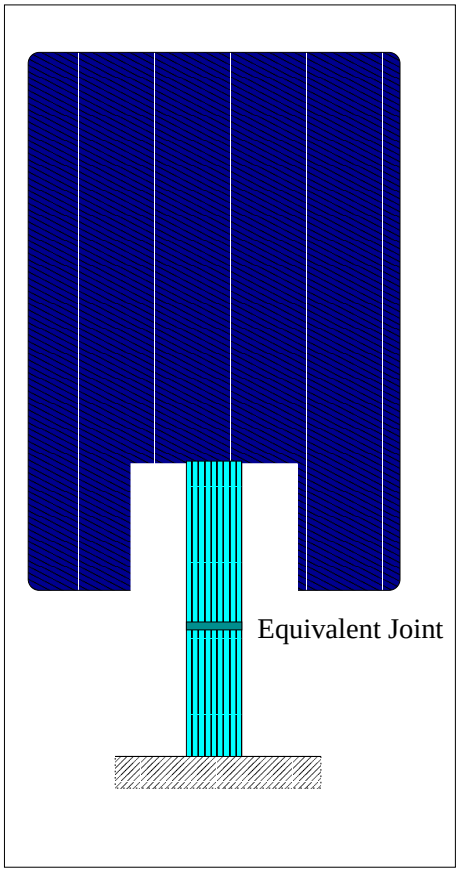

Figure 17. *Idealized joint orthogonal to the line of action of the applied forces: all joint forces and displacements are in the direction of the loads applied on the specimen.*

If we choose to account for the softness of the jointed leg through the compliance of the joint, we find the joint stiffness to be

$$K_T = \frac{1}{(1/K_J) - (1/K_M)} = \frac{1}{(1/2.67\text{x}10^6) - (1/1.56\text{x}10^6)} = 3.73\text{x}10^6\, lb_f/in \qquad (45)$$

Consideration of equilibrium shows the longitudinal force necessary to initiate macro-slip in the joint is

$$F_S = 504/\cos(45\,\text{deg}) = 712 \qquad (46)$$

Similarly, the the log-log dissipation versus force amplitude curves used to find the remaining parameters employs longitudinal force amplitudes that are $\sqrt{2}$ times the force amplitudes seen on the actual interface surface. Application of the Matlab code with and without reference to desired joint stiffness yields the parameters and fit shown in figure 18.

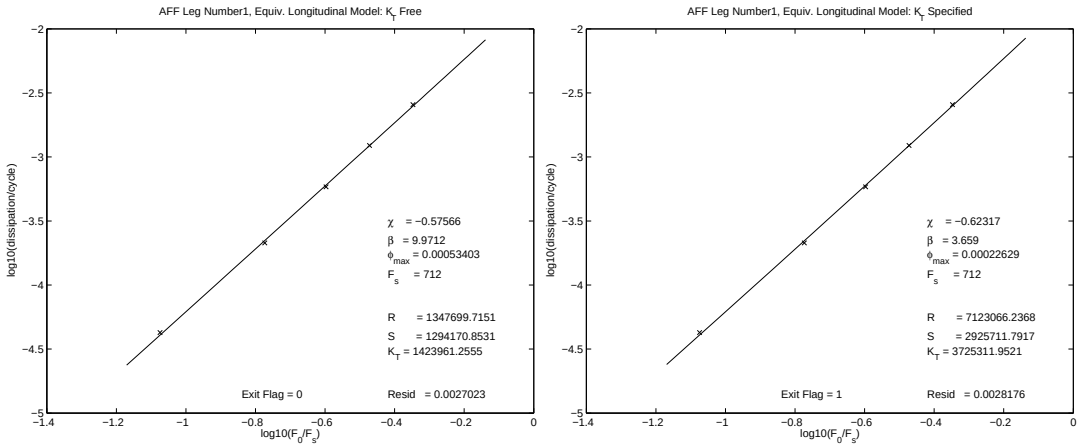

Figure 18. *Model fit for an idealized joint orthogonal to the line of action of the applied forces. A constraint on joint stiffness is imposed in the calculations indicated on the right and no such constraint is imposed in the calculations indicated on the left.*

As expected, we see that the additional constraint does result in the desired joint stiffness but does not significantly change the quality of fit of the model predictions to the experimental data points. Also as expected, though model parameters change, it is only β that changes significantly.

Discretization

Equations 6 and 7 are sufficient to solve for response of the above Iwan system once one has all system parameters (R, χ, β, and $\phi_{\max}$). It is useful to discretize the integral in Equation 6 in the following manner. One breaks up the interval $(0, \phi_{\max})$ into N intervals whose lengths form a geometric series:

$$\Delta\phi_{m+1} = \alpha\Delta\phi_m \quad \text{for all } m+1 < N \tag{47}$$

where α is a number slightly greater than one ($1 < \alpha$). That the sum of the intervals must be the whole interval:

$$\sum_{m=1}^{N} \Delta\phi_m = \phi_{\max} \tag{48}$$

permits us to solve

$$\Delta\phi_m = \alpha^{m-1}\Delta\phi_1 \tag{49}$$

where

$$\Delta\phi_1 = \left[\phi_{\max}\frac{\alpha-1}{\alpha^N-1}\right] \tag{50}$$

We consider one sample point, characterized by slide strength ϕ_m, at the mid-point of each interval $\Delta\phi_m$. At that sample point, the evolution of $x_m(t)$ is computed per Equation 7. For quadrature purposes, we refer to the coordinates of the left and right hand of each sub-interval as $\phi_{l,m}$ and $\phi_{r,m}$ respectively.

The force is evaluated by a discrete version of Equation 6.

$$F(t) = \sum_{m=1}^{N} F_m(t) + F_\delta(t) \tag{51}$$

where

$$F_m(t) = \begin{cases} R\,\frac{\phi_{r,m}^{2+\chi} - \phi_{l,m}^{2+\chi}}{2+\chi}\,\mathrm{sgn}[u(t) - x_m(t)] & \text{if } \|u(t) - x_m(t)\| = \phi_m \\ R\,\frac{\phi_{r,m}^{1+\chi} - \phi_{l,m}^{1+\chi}}{1+\chi}\,[u(t) - x_m(t)] & \text{if } \|u(t) - x_m(t)\| < \phi_m \end{cases} \tag{52}$$

$x_m(t)$ evolves per Equation 2 where $\phi = \phi_m$,

$$F_\delta = S\phi_{\max}[u(t) - x_\delta(t)], \tag{53}$$

and $x_\delta(t)$ evolves per Equation 2 where $\phi = \phi_{\max}$,

Note that the above quadrature reproduces the values for F_S in Equation 24 exactly.

The discretization discussed here is illustrated by the results of a C++ code that imposes cyclic deformation on a four-parameter Iwan system and calculates the energy dissipation once steady state is achieved (always on the second cycle). Those numerical calculations are compared with the analytic expressions of Equation 31. In Figure 19 we see that for the amplitude range $0.05F_S < F_0 < F_S$ integration over the responses of as few as ten Jenkins elements appears to be sufficient. We have achieved satisfactory simulations in all exercises using values of $\alpha = 1.2$ and $N = 50$. This is certainly overly conservative.

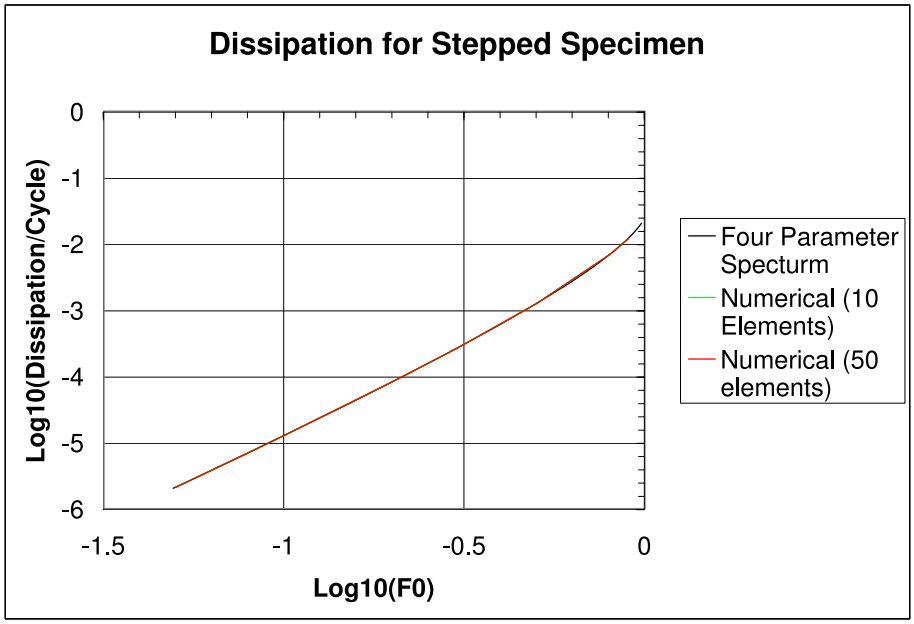

Figure 19. *Comparison of dissipation prediction of Equation 31 with the quadrature of Equations 51 through 53.*

The question arises as to over how many Jenkins elements we really must integrate. The simplest criteria are

- in a monotonic pull, the stiffness degradation from K_T down to zero at macroslip should occur without too much discontinuity in the stiffness slope:

$$\max_m \{\rho(\phi_m)\Delta\phi_m\} \ll K_T \tag{54}$$

where K_T is evaluated from Equation 29. The maximum term in the above

sequence is that associated with the last increment, so the condition is

$$R\left[\frac{\alpha^{N-1}(\frac{1+\alpha}{2})-1}{\alpha^N-1}\right]^{\chi}\frac{\alpha^{N-1}(\alpha-1)}{\alpha^N-1}\,\phi_{\max}^{1+\chi} \ll K_T \tag{55}$$

For large N, the product on the left behaves as a constant times $\alpha-1$. Values of α on the order of 1.1 or 1.2 appear to cause Equation 55 to be satisfied adequately.

- the sliding forces associated with the weakest element should slide at a force well below the smallest increment of force $\Delta F_{\min}$ between reversals that one wants to capture:

$$R\,\frac{\phi_{r,1}^{2+\chi}-\phi_{l,1}^{2+\chi}}{2+\chi} \ll \Delta F_{\min} \tag{56}$$

This becomes a condition that

$$R\left(\phi_{\max}\frac{\alpha-1}{\alpha^N-1}\right)^{\chi+2}/(\chi+2) \ll \Delta F_{\min} \tag{57}$$

The quantity on the left goes as $\alpha^{-(\chi+2)N}$, explaining why Equation 57 appears to be satisfied with fairly modest values of N.

Conclusion

The four-parameter model presented here appears to be capable of capturing the dissipation behavior found from harmonically loaded experiments on lap-type joints conducted so far. Further, the tools have been demonstrated to deduce the necessary model parameters with only modest effort.

Though the results presented here provide some reason for optimism, comparison with more sophisticated experiments should be made. Among those experiments could be multi-frequency experiments such as discussed by Segalman (2001) or random vibration experiments as performed by Smallwood for his hysteretic model. Each of these classes of experiment has been explored by Smallwood(2001) in connection with his power-law hysteresis model.

Finally, one should note that constitutive equations of the sort developed here are "whole-joint" models. Such models may capture the response of the joint for the class of loads from which model parameters were deduced, but they give little insight into the micro-physics taking place. Over that longer term, more sophisticated

approaches must be developed that better incorporate the tractions and displacements that develop dynamically around the joint and that do not presume a specific nature to the joint loading. An effort into that new direction has been initiated.

References

[1] M. Abromowitz and I. A. Stegun, *Handbook of Mathematical Functions, with Formulas, Graphs, and Mathematical Tables*, p. 1045, 1964

[2] W. D. Iwan, A Distributed-Element Model for Hysteresis and Its Steady-State Dynamic Response, *ASME Journal of Applied Mechanics, 33*, pp. 893-900, 1966

[3] W. D. Iwan, On a Class of Models for the Yielding Behavior of Continuous and Composite Systems, *ASME Journal of Applied Mechanics, 34*, pp. 612-617, 1967.

[4] M. B. Levine and C. White, Microdynamic Analysis for Establishing Nanometric Stability Requirements of Jointed Precision Space Structures, Paper No. 325, *Proceedings of the International Modal Analysis Conference* Kissimmee Fl., Feb. 2001.

[5] D. J. Segalman, *An Initial Overview of Iwan Modeling for Mechanical Joints*, SAND2001-0811, Sandia National Laboratories, Albuquerque, NM, March 2001.

[6] D. O. Smallwood, D. L. Gregory, and R. G. Coleman, A Three Parameter Constitutive Model for a Joint which Exhibits a Power Law Relationship Between Energy Loss and Relative Displacement, *72nd Shock and Vibration Symposium, Destin FL, Nov. 2001.* (Available from SAVIAC)

Example Matlab Files for Deducing Model Parameters

The following listings illustrate the automated approach to calculating model parameters. The code is invoked by first entering the Matlab environment and then reading in a file containing the experimental data:

```
AFF1_1
```

and reading in the fitting code

```
find_param
```

where the data code AFF1.m would have the following form:

```
%fitting AFF leg
verbage = 'AFF Leg Number1, Sample Set 1: Dissipation Data';
name = 'AFF1_1';
disp(verbage);


D=[42.42640687      4.25E-05
84.85281374     2.13E-04
127.2792206     5.84E-04
169.7056275     1.23E-03
226.27417       2.56E-03];

Fs= 504;
```

and the Matlab code find_param.m and the routines it calls are listed below.

find_param.m

```
%This routine should be invoked only after the experimental data is ...
%    read in.  This version permits consideration of a desired
%    stiffness K_T

force = D(:,1)/Fs;
Diss  = D(:,2);
N = length(force);

% If K_T is not an input parameter, signal that it should be ignored
% in determining model parameters.
if(exist('K_T') <1),
  K_T = -1;
end

% use optimizer to determine model parameters: \chi, \beta,
% \phi_max.  R is output as well for convenience.
%
[chi,R,phi_max,beta,resid,flag]=fit3(D,Fs,K_T);

% Joint stiffness and S are calculated from the above parameters.
K_Tr = R*(phi_max^(chi+1))*(1+beta)/(chi+1);
S = beta*(R*phi_max^(chi+1))/(chi+1);

chi_name  =       '\chi   ';
beta_name =       '\beta  ';
R_name =          'R      ';
S_name =          'S      ';
phi_max_name =    '\phi_{max}';
Fs_name =         'F_s    ';
K_T_name =        'K_T';
resid_name =      'Resid  ';
flag_name =       'Exit Flag';;

chi_val  =       num2str(chi);
beta_val =       num2str(beta);
R_val =          num2str(R);
S_val =          num2str(S);
phi_max_val =    num2str(phi_max);
```

```
Fs_val =         num2str(Fs);
K_T_val   =      num2str(K_Tr);
resid_val =      num2str(resid);
flag_val =       num2str(flag);

chi_val_Eq      =       [chi_name,      ' = ', chi_val];
beta_val_Eq     =       [beta_name,     ' = ', beta_val];
R_val_Eq        =       [R_name,        ' = ', R_val];
S_val_Eq        =       [S_name,        ' = ', S_val];
phi_max_val_Eq  =       [phi_max_name,  ' = ', phi_max_val];
Fs_val_Eq       =       [Fs_name,       ' = ', Fs_val];
K_T_val_Eq       =      [K_T_name,       ' = ', K_T_val];
resid_val_Eq    =       [resid_name,    ' = ', resid_val];
flag_val_Eq    =        [flag_name,     ' = ', flag_val];

disp(chi_val_Eq);
disp(beta_val_Eq);
disp(R_val_Eq);
disp(S_val_Eq);
disp(phi_max_val_Eq);
disp(Fs_val_Eq);
disp(K_T_val_Eq);
disp(resid_val_Eq);
disp(flag_val_Eq);

% Plot these results
rmin = 0.8*find_r(force(1),chi,beta);
rmax=  (find_r(force(N),chi,beta)+1)/2;
Points = 51;

for i=1:Points,
  eps =  (i-1)/(Points-1);
  r(i) = rmin + eps*(rmax-rmin);
  Fr(i) =   r(i)*( (beta+1)-(r(i)^(chi+1))/(chi+2) )/ ...
  ( beta+(chi+1)/(chi+2) );
  Dr(i) = 4*R*((r(i)*phi_max)^(chi+3))/( (chi+2)*(chi+3) );
end

%save these comparision data
comp_file_name = [name, '.mat'];
```

```
eval(['save ',comp_file_name,' chi beta phi_max Fs force Diss Fr Dr ']);

plot(log10(force),log10(Diss),'x',log10(Fr), log10(Dr));
% axis( [log10(force(1)), log10(force(length(force))), ...
%       log10(Diss(1)), log10(Diss(length(force)))])
title(verbage);
xlabel('log10(F_0/F_s)');
ylabel('log10(dissipation/cycle)');

text(0.7,0.5,  chi_val_Eq,    'sc');
text(0.7,0.45, beta_val_Eq,   'sc');
text(0.7,0.40, phi_max_val_Eq,'sc');
text(0.7,0.35, Fs_val_Eq,     'sc');

text(0.7,0.25, R_val_Eq,  'sc');
text(0.7,0.20, S_val_Eq,  'sc');
text(0.7,0.15, K_T_val_Eq,'sc');

text(0.7,0.05, resid_val_Eq,'sc');
text(0.4,0.05, flag_val_Eq, 'sc');


printname = [name,'.ps'];
eval(['print -dpsc ',printname]);

outname = [name,'.out'];
fout = fopen(outname, 'w');
%First Identify data set, then put out fitted values
fprintf(fout, '\t%s\n', name);
fprintf(fout, '%s \t %s\n', chi_name,    chi_val);
fprintf(fout, '%s \t %s\n', beta_name,   beta_val);
fprintf(fout, '%s \t %s\n', phi_max_name,phi_max_val);
fprintf(fout, '%s \t %s\n', Fs_name,     Fs_val);
fprintf(fout, '%s \t %s\n', R_name,      R_val);
fprintf(fout, '%s \t %s\n', S_name,      S_val);
fprintf(fout, '%s \t %s\n', resid_name,  resid_val);
fprintf(fout, '%s \t %s\n', flag_name,   flag_val);
fprintf(fout, '\n');
fclose(fout);
```

fit3.m

```
%
%  [chi,R,phi_max,beta,resid,flag]=fit3(Din,Fs,K_T);
%
%   where Din = [force dissipation] (n x 2) matrix
%         Fs = breakfree force
%
function [chi,R,phi_max,beta,resid,flag]=fit3(Din,Fs,K_T)
N = length(Din);
force = Din(:,1)/Fs;
Diss  = Din(:,2);

% first guesses for parameters
chi = 0.0;
R = median(Diss);
phi_max = 1.0e-5;
beta =5;

if size(Din,1)<2,
  disp('pls provide at least 2 points');
else
  p=zeros(2*N+2,1);
  % why is this dimensioned to N instead of 3
  x=zeros(3,1);
  for i=1:N,
    p(i)   = force(i);
    p(i+N) = Diss(i);
  end
  p(2*N+1) = Fs;
  p(2*N+2) = K_T;

  x(1) =  chi;          % first guess for chi
  x(2) =  beta;         % first guess for beta
  x(3) =  R;            % first guess for R_p3c

  options = optimset('TolX',1e-5,'Display','final');
  [x,resid,flag]=fminsearch('para_fit3',x,options,p);

  chi   = x(1);
```

```
  beta  = x(2);
  R_p3c = x(3);          %this should be R*phi_max^(chi+3)

  r = zeros(N,1);

  % estimate phi_max from each experimental data pair
  pm = zeros(N,1);

  for i=1:N,
      r(i) = find_r(force(i), chi, beta);
      pm(i) = (Diss(i)/Fs)*( (chi+3)*(beta+(chi+1)/(chi+2)) )/ ...
    (4*(r(i)^(chi+3))*(chi+1)/(chi+2));
  end

  % average these to get a nominal phi_max
  phi_max = sum(pm)/N;

  R = R_p3c/phi_max^(chi+3);

end
```

para_fit3.m

```
function [err]=para_fit3(x,p)

% there are N data points
N = floor(length(p)/2)-1;
F = zeros(N,1); % dimensionless force
D = zeros(N,1); % dissipation at each data point
r = zeros(N,1); % estimate for r corresponding to each F

for i=1:N,
  F(i)=p(i);
  D(i)=p(i+N);
end
Fs  = p(2*N+1);
K_T = p(2*N+2);

chi   = x(1);
beta  = x(2);
R_p3c = x(3);

% for each data point force F and current values for chi & beta
% calculate the corresponding r

for i=1:N,
  r(i) = find_r(F(i), chi, beta);
end

%calculate the corresponding dissipation
y=zeros(N,1);
for i=1:N,
  y(i) = 4*R_p3c*(r(i)^(chi+3))/( (chi+2)*(chi+3) );
end


res = zeros(N,1);
for i=1:N,
  %  res(i) =  (y(i)-D(i))/D(i);
  res(i) =  log10(y(i)/D(i));
end
```

```
%net residual
err =   res'*res ;

% calculate stiffness
phi_max = (R_p3c/Fs)*(beta + (chi+1)/(chi+2))/(chi+1);
R = R_p3c/phi_max^(chi+3);
K_Tr = R*(phi_max^(chi+1))*(1+beta)/(chi+1);

if((1.0e-5< K_T) & (1<beta))
  err = err + ((K_T - K_Tr)/K_T)^2;
end

%TEST TEST
%weight toward smaller magnitude chi
err = err + (5.0e-3)*chi*chi;

%Try to bound beta & chi
if(10<beta),
  err = err + 1.0e3*(beta-10)^2;
end
if(beta<0.001),
  err = err + 1.0e6*(beta-0.001)^2;
end


if(chi<-0.999),
  err = err + 1.0e6*(chi+0.999)^2;
end
```

find_r.m

```
%
% r = find_r(Ft,chi,beta);
%
% routine to find the r that results in a target value of Ft
%
function r = find_r(Ft, chi, beta)
%
%
% first estimate:
r = Ft;
%
% iteration parameters
i = 1; max_i = 100;
tol = 1.0e-4;
res = Ft;
while (i<max_i & Ft*tol<abs(res))
  F = r*( (beta+1)-(r^(chi+1))/(chi+2) )/ ...
   ( beta+(chi+1)/(chi+2) );
  res = F-Ft;
  slope = ( (beta+1) - r^(chi+1) )/(beta + (chi+1)/(chi+2));
  r = r - res/slope;
  r = max(r, -1);
  r = min(r, 1);
  i = i+1;
end
```

DISTRIBUTION:

5 Prof. Lawrence A. Bergman
University of Illinois
306 Talbot Lab
104 S. Wright St.
Urbana, IL 61801

1 Dr. Scott Doebling
Los Alamos National Laboratory, MS P946
Los Alamos, NM 87545

1 Dr. Steve Griffin
Boeing SVS
4411 The25 Way NE
Suite 350
Albuquerque, NM 87109

1 Dr. Jason Hinkle
Aerospace Engineering Sciences
Campus Box 429
University of Colorado
Boulder, CO 80309-0429

1 Prof. Raouf A. Ibrahim
College of Engineering
2119 Engineering Bldg.
Mechanical Engineering Department
Wayne State University
Detroit, MI 48202

1 Dr. Marie Levine-West
Jet Propulsion Laboratory
Science and Technology Development Section
4800 Oak Grove Drive
Pasadena, CA 91109-8099

1 Professor K. C. Park
College of Engineering and Applied Science
University of Colorado
Boulder, CO 80309-0429

1 Prof. Lee Peterson
Aerospace Engineering Sciences
Campus Box 429
University of Colorado
Boulder, CO 80309-0429

1 Dr. Chris Pettit
AFRL/VASD,
Bldg. 146, 2210 Eighth St.,
Wright Patterson AFB
OH 45433

1 Prof. D. Dane Quinn
Department of Mechanical Engineering
College of Engineering
The University of Akron
107b Auburn Science and Engineering Center
Akron, OH 44325-3903

1 Dr. Y.C. Yiu
Lockheed Martin Missiles & Space
Organization E4-20 Bldg 154
1111 Lockheed Martin Way
Sunnyvale, CA 94089

1 MS 191
Epp, David S , 9125

1 MS 191
Ozdoganlar, O Burak , 9124

1 MS 553
Bateman, Vesta I , 9126

1 MS 553
Smallwood, David O , 9124

1 MS 555
Garrett, Mark S , 9122

1 MS 555
Gregory, Danny L , 9122

1 MS 555
Hansche, Bruce D , 9122

1 MS 555
Nelson, Curtis F , 9124

1 MS 555
Nusser, Michael A , 9122

1 MS 557
Baca, Thomas J , 9125

1 MS 557
Carne, Thomas G , 9124

1 MS 557
Larkin, Paul A , 9125

1 MS 557
Mayes, Randall L , 9125

1 MS 557
O'Gorman, Christian C , 9125

1 MS 557
Paez, Thomas L , 9133

1 MS 557
Simmermacher, Todd W , 9124

1 MS 557
Urbina, Angel , 9133

1 MS 821
Gritzo, Louis A , 9132

1 MS 824
Moya, Jaime L , 9130

1 MS 824
Ratzel, Arthur C , 9110

1 MS 828
Pilch, Martin , 9133

1 MS 834
Johannes, Justine E , 9114

1 MS 835
McGlaun, J Michael , 9140

1 MS 835
Naething, Richard M , 9142

1 MS 835
Pierson, Kendall Hugh , 9142

1 MS 835
Walsh, Timothy Francis , 9142

1 MS 841
Bickel, Thomas C , 9100

1 MS 841
Peterson, Carl W , 9100

1 MS 847
Alvin, Kenneth F , 9124

1 MS 847
Attaway, Stephen W , 9134

1 MS 847
Bhardwaj, Manoj K , 9142

1 MS 847
Bitsie, Fernando , 9124

1 MS 847
Blanford, Mark L , 9142

1 MS 847
Burchett, Steven N , 9126

1 MS 847
Dohrmann, Clark R , 9124

1 MS 847
Duong, Henry , 9126

1 MS 847
Fulcher, Clay W G , 9125

1 MS 847
Gwinn, Kenneth W , 9126

1 MS 847
Heinstein, Martin W , 9142

1 MS 847
Hinnerichs, Terry , 9126

1 MS 847
Hopkins, Ronald N , 9125

1 MS 847
Jung, Joseph , 9126

1 MS 847
Lash, Joel , 9126

1 MS 847
May, Rodney A , 9126

1 MS 847
Mitchell, John A , 9142

1 MS 847
Morgan, Harold S , 9120

1 MS 847
Red-Horse, John R , 9133

1 MS 847
Redmond, James M , 9124

1 MS 847
Reese, Garth M , 9142

10 MS 847
Segalman, Daniel J , 9124

1 MS 847
Sumali, Hartono , 9124

1 MS 847
Walther, Howard P , 9125

1 MS 847
Wojtkiewicz, Steven F Jr , 9124

1 MS 893
Brannon, Rebecca M , 9123

1 MS 893
Lo, Chi , 9123

1 MS 893
Reedy, Dave , 9123

1 MS 1110
Day, David M. , 9214

1 MS 1023
Stasiunas, Eric Carl , 9124

1 MS 1080
Dohner, Jeffrey L, 1769

1 MS 1135
Coleman, Ronald G , 9122

1 MS 1360
Resor, Brian R , 9122

1 MS 1393
Chu, Tze Yao , 9100

1 MS 9018
Central Technical Files, 8945-1

2 MS 0899
Technical Library, 9616

1 MS 0612
Review & Approval Desk, 9612